INFLUENCE OF LA IN xPBBIN OF TERNARY NANOCERAMIC COMPOSITE (1-x)0.5PMN-0.5PZT-xPBBiN SYSTEM BY MECHANICAL ACTIVATION TECHNIQUE FOR DIELECTRIC AND PIEZOELECTRIC PROPERTIES

KODURI RAMAM[#], K. CHANDRAMOULI*

Departmento de Ingenieria de Materials, (DIMAT), Facultad de Ingenieria, Universidad de Concepcion, Concepcion, Chile
**Solid State Physics and Materials Research Laboratory, Department of Physics, Andhra University, Visakhapatnam, India*

[#]E-mail: ramamk@udec.cl

Submitted November 8, 2010; accepted May 8, 2011

Keywords: Ferroelectrics; X-ray diffraction; Dielectric response; Mechanical Activation, Piezoelectricity

(1-x)[0.5Pb($Mg_{0.33}Nb_{0.67}$)O_3-0.5Pb($Zr_{0.53}Ti_{0.47}$)O_3]-x[$Pb_{0.557}Ba_{0.38}La_{0.022}Bi_{0.02}Nb_2O_6$] with both perovskite and tungsten bronze structured composite have been synthesized through mechanical activation technique. The strong influence of lanthanum addition to the lead-barium-bismuth-niobate (xPBLBiN) ceramics in perovskite structured (1-x)PMN-PZT on structural and functional properties is confirmed. X-ray diffraction patterns studies showed that these complex composites consisted of perovskite Cubic with tungsten bronze Orthorhombic phases. La modification in PBBiN of a ternary system (1-x)PMN-PZT-xPBBiN revealed intensified orthorhombicity. As La increased the dielectric and piezoelectric properties tremendously increased in (1-x)PMN-PZT-xPBLBiN nanoceramic composite. The optimum dielectric and piezoelectric properties (ε_{RT} = 2931, k_p = 0.461 and d_{33} = 428 pC/N) were found in x =0.4 composite. We achieved novel nanocomposites synthesized by high energy ball milling method and having binary structures in a single composite with excellent functional properties that can be used for energy harvesting applications.

INTRODUCTION

Lead Magnesium Niobate-Lead Zirconium Titanate (PMN-PZT) belongs to perovskite group having ABO_3 structure and Lead Barium Bismuth Niobate (PBBiN) belongs to tungsten bronze group with a BO_6 structure. The perovskite system exhibits a morphotrophic phase boundary between rhombohedral and tetragonal phases at 53:47 Zr/Ti ratios whereas tungsten bronze system exhibits a morphotrophic phase boundary between orthorhombic and tetragonal phases at x = 0.63 where the dielectric and piezoelectric properties are enhanced [1-3]. The orthorhombic symmetry (O) can be represented as *mm2* or *m2m* depending on the polarization rotation. The tetragonal symmetry (T) can be represented as *4mm*. The trigonal or rhombohedral symmetry (R) can be represented as *3m*. The hexagonal symmetry (H) can be represented as *6mm*. The paraelectric tetragonal symmetry can be represented as *4/mmm* and cubic symmetry can be represented as *m3m* [4]. In PZT ceramics, Zr rich compositions are rhombohedral and Ti rich compositions are tetragonal while in PBN ceramics, Pb rich compositions are orthorhombic and Ba rich compositions are tetragonal. PMN-based, PZT-based, PBN-based, PMN-PZT based and several other Pb-based ternary systems have been extensively investigated. However, there has been no study on the combination of PMN-PZT-PBBiN ternary system up to date. Moreover, La modification in the PMN-PZT-PBBiN ternary system has not been reported in the literature.

Several investigations have been studied on different ferroelectric compounds through high-energy mechanical activation process; PT [5], PLZT [6], PZN [7], PFW [8], $Bi_3T_4O_{12}$ [9], $BaTiO_3$, $Bi_{0.5}Na_{0.5}TiO_3$ and $Ba_2NaNb_5O_{15}$ [10], PMN [11], PMN-PT [12] etc. We have reported the functional properties (1-x)PMN-PZT-xPBBiN synthesized through mechanical activation route [13]. The addition of rare earths provides a fine control of the physical properties. It is reported that La^{3+} doped PBN ceramics showed high electro-optic coefficients and decreases the Curie temperature [14]. On the other hand, Neurgaonkar et al. [15] studied La^{3+} modified PBN60 ceramics which showed 6 mol% La reduces the spontaneous polarization. Further, detailed literature survey shows that no work has been reported on ternary system of La modified (1-x)PMN-PZT-xPBBiN ceramic composite through mechanical activation technique. In this work, La modification in PBBiN ceramic composite

in a ternary system (1-x)PMN-PZT-xPBBiN was studied in order to investigate the composition range for the formation of the orthorhombic phase caused by the La^{3+} doping and to study its structural and functional properties on account of the tremendous potential of Pb-based electroceramics.

EXPERIMENTAL

Synthesis of (1-x)(0.5PMN-0.5PZT)-xPBLBiN nanoceramic complex composite system

Analytical reagent grade (99.99% purity) starting materials (PbO, MgO, ZrO_2, TiO_2, $BaCO_3$, Bi_2O_3, La_2O_3 and Nb_2O5 (Sigma Aldrich, USA) were subjected to high energy mechanical activation milling to obtain (1-x)(0.5PMN-0.5PZT)-xPBLBiN composite: (1-x)[0.5Pb$(Mg_{0.33}Nb_{0.67})O_3$-0.5Pb$(Zr_{0.53}Ti_{0.47})O_3$]-x[$Pb_{0.557}Ba_{0.38}La_{0.022}Bi_{0.02}Nb_2O_6$]. Please refer Table 1**.** The synthesis was carried out using Fritsch Pulverisette 5 high-energy ball milling system. Appropriate amounts of the constituent oxides as per the stoichiometric compositions were mixed together and milled in a 250 ml agate bowl with high wear resistant Zirconia grinding media. The balls were 3 mm in diameter, and the ball to powder ratio was 10:1 and milling was carried out in toluene medium. Milling was done at a speed of 250 rpm for 20 h. The milling was stopped for 5 min after every 30 min of milling to cool down the system. The milled powders were calcined at 900°C for 2 h. Calcined batch powders were ground for crushing agglomerates and 5wt% PVA binder was added, and subsequently powders were pressed into pellets of 12mm in diameter and 2mm thickness, using a steel die and uniaxial hydraulic cold press with pressures of 700–900 kg/cm^2. The green bodies were sintered at 1050°C for 2 h in a high temperature furnace.

Structural characterization of (1-x)(0.5PMN-0.5PZT) -xPBLBiN nanoceramic complex composite system

The phase formation in the nanocomposites were analyzed by powder X-ray diffraction (XRD) technique (Philips X-ray diffractometer PW-1710) using CuK_α radiation with Ni filter at room temperature and a step scan from 2q = 20 to 60°. JEOL JSM 840A scanning electron microscopy was used to analyze microstructure of polished, etched and sintered fractured ceramic surfaces. The morphology of nanoparticles was observed by JEOL TEM 1200 transmission electron microscope. Densities of sintered batch samples were measured by Archimedes method.

Electrical characterization of (1-x)(0.5PMN-0.5PZT) -xPBLBiN nanoceramic complex composite system

Polished and silver electroded specimens were characterized for temperature dependent dielectric response by using HP 4192A impedance analyzer and a pro-

Table 1. (1-X)(pmn-pzt)-xPBLBIN nanoceramic composites..

Composition	Formulae
General formula (1-x)(0.5PMN-0.5PZT)-xPBBiN	(1-x)[0.5Pb$(Mg_{1/3}Nb_{2/3})O_3$-0.5Pb$(Zr_{0.53}Ti_{0.47})O_3$]-x[$Pb_{(1-b-(3k/2)-(3m/2))}Ba_bLa_kBi_mNb_2O_6$]
Stoichiometric Formula	(1-x)[0.5Pb$(Mg_{0.33}Nb_{0.67})O_3$-0.5Pb$(Zr_{0.53}Ti_{0.47})O_3$]-x[$Pb_{0.557}Ba_{0.38}La_{0.022}Bi_{0.02}Nb_2O_6$]
	where x = 0,0.2,0.4,0.6,0.8,1, Zr/Ti ratio = 53:47, Ba = b = 38 mol%, La = k = 2.2 mol% and Bi = z = 2 mol%
PMN-PZT	$[(0.5)PbO0.3333MgO0.6667Nb_2O_5$-$(0.5)PbO0.53ZrO_20.47TiO_2] \rightarrow [0.5Pb(Mg_{0.33}Nb_{0.67})O_3$-$0.5Pb(Zr_{0.53}Ti_{0.47})O_3]$
(0.8)[0.5PMN-0.5PZT]-(0.2)PBLBiN	$0.8[(0.5)PbO0.3333MgO0.6667Nb_2O_5$-$(0.5)PbO0.53ZrO_20.47TiO_2]+0.2[0.557PbO+0.38BaCO_3+0.011La_2O_3+0.01Bi_2O_{3+}Nb_2O_5] \rightarrow$ $(0.8)[0.5Pb(Mg_{0.33}Nb_{0.67})O_3$-$0.5Pb(Zr_{0.53}Ti_{0.47})O_3]$- $0.2[Pb_{0.557}Ba_{0.38}La_{0.022}Bi_{0.02}Nb_2O_6]+0.076CO_2\uparrow$
(0.6)[0.5PMN-0.5PZT]-(0.4)PBLBiN	$0.6[(0.5)PbO0.3333MgO0.6667Nb_2O_5$-$(0.5)PbO0.53ZrO_20.47TiO_2]+ 0.4[0.557PbO+0.38BaCO_3+0.011La_2O_3+0.01Bi_2O_{3+}Nb_2O_5] \rightarrow$ $(0.6)[0.5Pb(Mg_{0.33}Nb_{0.67})O_3$-$0.5Pb(Zr_{0.53}Ti_{0.47})O_3]$-$0.4[Pb_{0.557}Ba_{0.38}La_{0.022}Bi_{0.02}Nb_2O_6]+0.152CO_2\uparrow$
(0.4)[0.5PMN-0.5PZT]-(0.6)PBLBiN	$0.4[(0.5)PbO0.3333MgO0.6667Nb_2O_5$-$(0.5)PbO0.53ZrO_20.47TiO_2]+ 0.6[0.557PbO+0.38BaCO_3+0.011La_2O_3+0.01Bi_2O_{3+}Nb_2O_5] \rightarrow$ $(0.4)[0.5Pb(Mg_{0.33}Nb_{0.67})O_3$-$0.5Pb(Zr_{0.53}Ti_{0.47})O_3]$- $0.6[Pb_{0.557}Ba_{0.38}La_{0.022}Bi_{0.02}Nb_2O_6]+0.228CO_2\uparrow$
(0.2)[0.5PMN-0.5PZT]-(0.8)PBLBiN	$0.2[(0.5)PbO0.3333MgO0.6667Nb_2O_5$-$(0.5)PbO0.53ZrO_20.47TiO_2]+ 0.8[0.557PbO+0.38BaCO_3+0.011La_2O_3+0.01Bi_2O_{3+}Nb_2O_5] \rightarrow$ $(0.2)[0.5Pb(Mg_{0.33}Nb_{0.67})O_3$-$0.5Pb(Zr_{0.53}Ti_{0.47})O_3]$-$0.8[Pb_{0.557}Ba_{0.38}La_{0.022}Bi_{0.02}Nb_2O_6]+0.304CO_2\uparrow$
PBLBiN	$[0.557PbO+0.38BaCO_3+0.0.011La_2O_3+0.01Bi_2O_{3+}Nb_2O_5] \rightarrow [Pb_{0.557}Ba_{0.38}La_{0.022}Bi_{0.02}Nb_2O_6]+0.38CO_2\uparrow$

grammable furnace. The electroded specimens were poled in silicon oil bath at 100°C by applying a dc field of 20kV/cm. After 24 h ageing, the poled specimens were characterized for piezoelectric studies. The piezoelectric charge coefficient (d_{33}) was characterized by using a Berlincourt piezo-d-meter. The piezoelectric planar coupling coefficient (k_p) was characterized through resonance and anti-resonance technique by using a 4192A HP impedance analyzer.

RESULTS AND DISCUSSION

Figure 1 depicts X-ray diffraction patterns of (1-x)(0.5PMN-0.5PZT)-xPBLBiN nanoceramic composites. The X-ray diffraction patterns showed coexistence of Cubic perovskite PMN and orthorhombic PBLBiN. As x concentration increased, Cubic perovskite structure has been modified with orthorhombic PBLBiN in forming in-situ composite ceramic system. We have reported the optimization process (1-x)PMN-PZT-xPBBiN synthesized through mechanical activation route in our previous investigations [13]. Based on the optimized conditions, we have considered Fritsch Pulverisette planetary milling process at a speed of 250 rpm for 20h. The in-situ prepared composite through mechanical alloying technique with 20 h at a speed of 250 rpm was pyrochlore-free due to lowering of processing temperatures. The PBN solid solution phase diagram has a vertical line at 1-x ~ 0.63 that separates the two ferroelectric phases, orthorhombic (*mm2* or *m2m*) and tetragonal (*4mm*). In the orthorhombic ferroelectric phase, the spontaneous polarization P_s is along one of the 2-fold axes (001)p (of point group *mm2*) or (110)p (denoted as point group *m2m*) where the suffix indicates that the orientation refers to the original prototypic axial system, while on the tetragonal (*4mm*) phase, the polar axis is along (001) direction. Generally, the orthorhombic unit cell is a ¹ b ¹ c and tetragonal unit cell is a ¹ c. In the barium-rich region, it is tetragonal *4mm* structure with only 180° domains. In the lead-rich region, PBN has an orthorhombic *m2m* or *mm2* structure with both 180° and 90° domains [16]. In our study, La influenced the orthorhombicity in xPBBiN due to the existence of both 180° and 90° domains and different ionic radii of different cations make them preferentially distributed in A-sites and B-sites. Please refer Table 2. It is reported in the literature that a similar study of (1-x)$Ba_{0.4}Na_{0.2}NbO_3$-x$Pb(Mg_{1/3}Nb_{2/3})O_3$ system showed coexistence of three phases viz. $Ba_2NaNb_5O_{15}$ (BNN), $Pb(Mg_{1/3}Nb_{2/3})O_3$ (PMN) and pyrochlore in the sample x=0.4~0.6 composite [**17**]. Whilst in our study, we synthesized the ternary system and achieved pyrochlore-free PMN-PZT-PBBiN nanocomposites. The coexistence of perovskite cubic (1-x)PMN-PZT and tungsten bronze orthorhombic xPBLBiN were the evident phases and the crystallinity further enhanced with increasing La in xPBBiN up to x = 0.4. The orthorhombic tungsten bronze phase became predominant in x = 1.0 in the series.

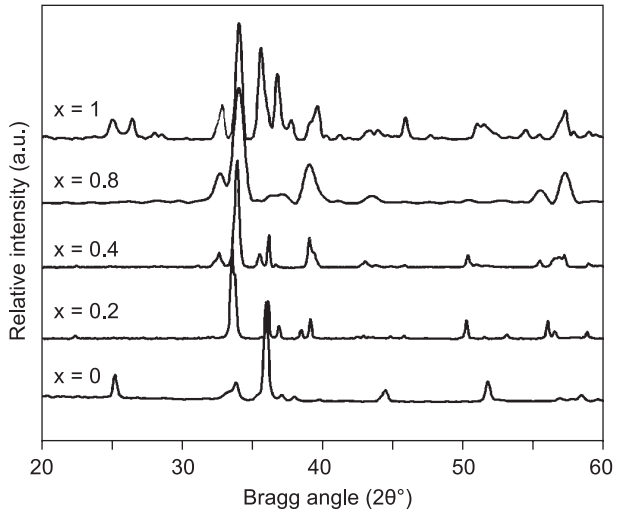

Figure 1. X-ray diffraction patterns of (1-x)(0.5PMN-0.5PZT) -xPBLBiN nanoceramic composites.

Figure 2 shows the scanning electron micrograph of sintered and fractured 0.8(0.5PMN-0.5PZT)-0.2PBLBiN and 0.6(0.5PMN-0.5PZT)-0.4PBLBiN nano-ceramic composites. Figure 3 shows trans-

Table 2. (1-x)(PMN-PZT)-xPBLBiN ionic radii.

Composition	Cation	Structure	Fold (Coordination Number)	Ionic Radii (Å)	Site
(1-x) PMN-PZT	Pb^{2+}	Perovskite	12	1.49	A-site
	Mg^{2+}	Perovskite	6	0.72	B-site
	Nb^{5+}	Perovskite	6	0.64	B-site
	Zr^{4+}	Perovskite	6	0.72	B-site
	Ti^{4+}	Perovskite	6	0.605	B-site
xPBLBiN	Pb^{2+}	Tungsten Bronze	12 (Square)	1.49	$(A1\text{-sites})_2$
	Ba^{2+}	Tungsten Bronze	15 (Pentagon)	1.61	$(A2\text{-sites})_4$
	La^{3+}	Tungsten Bronze	12 (Square)	1.36	$(A1\text{-sites})_2$
	Bi^{3+}	Tungsten Bronze	12 (Square)	1.03	$(A1\text{-sites})_2$
	Excess (if any)	Tungsten Bronze	9 (Triangle)		$(C\text{-sites})_4$/empty
	Nb^{5+}	Tungsten Bronze	6	0.64	$(B1\text{-sites})_2$ $(B2\text{-sites})_8$

mission electron micrograph of 0.6(0.5PMN-0.5PZT) -0.4PBLBiN nanoceramic composite. In this nanocomposite system, as x increased the apparent density increased till x = 0.4 and then decreased. The density of these nanoceramic composites ranged from x = 0 (7.48 gm/cm^3) to x = 1 (7.51 gm/cm^3). The density of sintered ceramics, as measured by Archimedes' principle was found to be >98% of the theoretical density for the given nanocomposites. It is speculated that the TB-grain growth supported perovskite granular growth. The increased trend till x = 0.4 (7.57 gm/cm^3) is due to (a) well grown closely packed perovskites-tungsten bronze grains, (b) pyrochlore-free tungsten bronze phase (from XRD studies), (c) nano powders assisted the densification process and (d) multiple cations existing at A-site and B-site of both perovskite and tungsten bronze structures, and the decreasing trend till x = 1.0 can be attributed to lanthanum increment which affects the density. The average crystallite size observed ranged from 21 to 48 nm, indicating the successful reduction of particle size as an outcome of mechanically milling the powders. The fractured ceramic surfaces indicated sub-micron grain growth. Microstructure of the samples sintered at 1050°C for 2 h as a function of x (PBLBiN) were homogenous in nature. The elongated grain growth can be attributed to ionic diffusion between the two distinct perovskite and tungsten bronze structures, respectively. The grains are elongated and uniformly distributed over the entire surface with a closely packed microstructure. The La addition in PBBiN accelerated the grain growth and improved the densification in the nanoceramic composite system. It is observed that high energy mechanical activation milling process supported the microstructure. It is reported that BNN and PMN contributed low densification due to filled TB structure and ionic diffusion in the structure was not easier unlike other TB structures containing empty sites. They also reported that some extent of grain growth was not observed due to the pyrochlore phase which suppressed grain growth [18]. Whilst in our study, we achieved binary phases of perovskite cubic PMN-PZT and tungsten bronze orthorhombic PBLBiN with no traces of pyrochlore which can be attributed to mechanical activation technique.

Figure 4 shows the dielectric properties of (1-x) (0.5PMN-0.5PZT)-xPBLBiN nanoceramic composites. It is observed that dielectric constant increased up to x = 0.4 and was found to be optimum. The ternary system in the nanocomposite system PMN-PZT-PBLBiN influenced the cationic polarization and enhanced the domain wall movement due to multiple ions in the lattice. The relaxor electrostrictive PMN and ferroelectric PZT together with ferroelectric tungsten bronze PBLBiN could have contributed to the increase of dielectric properties. It is evident that the binary structures in the (1-x)(0.5PMN-0.5PZT)-xPBLBiN ternary nanoceramic composite with intensified orthorhombic phase due to Pb-rich composition and introduction of La and Bi in tungsten bronze system can be attributed to the enhanced dielectric properties. The dielectric loss ($Tand_{RT}$) and

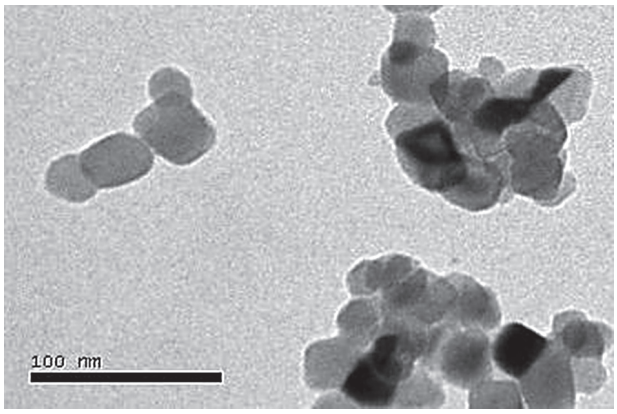

Figure 3. Transmission electron micrograph of 0.6(0.5PMN -0.5PZT)-0.4PBLBiN nanoceramic composite.

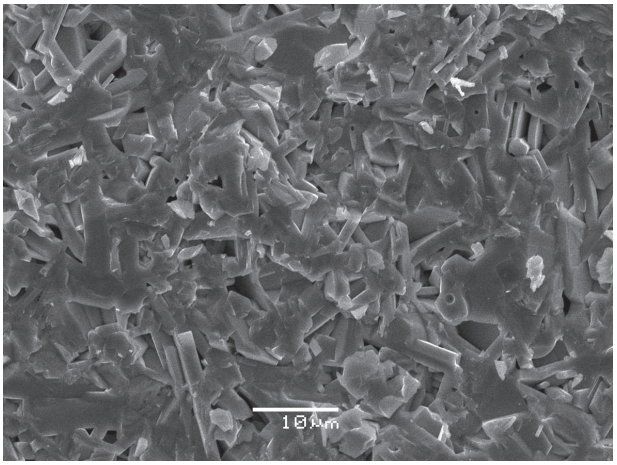

a) x = 0.2

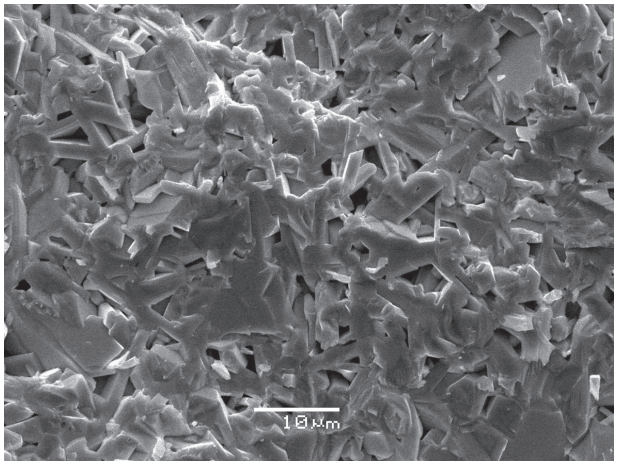

b) x = 0.4

Figure 2. Scanning electron micrograph of sintered and fractured 0.8(0.5PMN-0.5PZT)-0.2PBLBiN and 0.6(0.5PMN-0.5PZT) -0.4PBLBiN nanoceramic composites.

Curie temperature followed decreasing trend throughout the system which could be attributed to La addition. The microstructure evolution and electrical properties of tungsten bronze $Ba_2NaNb_5O_{15}$ and perovskite $Pb(Mg_{1/3}Nb_{2/3})O_3$ composites prepared through solid state reaction method was reported. They observed that small amounts of BNN resulted in more dispersed dielectric transition caused by compositional inhomogeneity and Na induced disordering of PMN [19]. On the contrary, in our study, the optimum dielectric properties (e_{RT} = 2931) were observed in x = 0.4 and we obtained both compositional and microstructural homogeneity in (1-x)(0.5PMN-0.5PZT)-xPBLBiN nanoceramic composites.

Figure 5 depicts piezoelectric properties (piezoelectric charge coefficient, d_{33} and piezoelectric planar coupling coefficient, k_p) of (1-x)(0.5PMN-0.5PZT) -xPBLBiN nanoceramic composites. The piezoelectric charge coefficient (d_{33}) and piezoelectric planar coupling coefficient (k_p) exhibited optimum values (k_p = 0.461 and d_{33} = 428 pC/N) at x = 0.4 in (1-x)(0.5PMN-0.5PZT) -xPBLBiN nanoceramic composites. The nanoceramic composites having both perovskite cubic and tungsten bronze orthorhombic structures as well as La addition to tungsten bronze structure increased the piezoelectricity. It is well known that small amounts of La drastically increase the electromechanical properties as piezoelectric properties are influenced by dopant concentrations and the preparation technique. In our study, La influenced the orthorhombicity in xPBBiN due the existence of both 180° and 90° domains and different ionic radii of different cations make them preferentially distributed

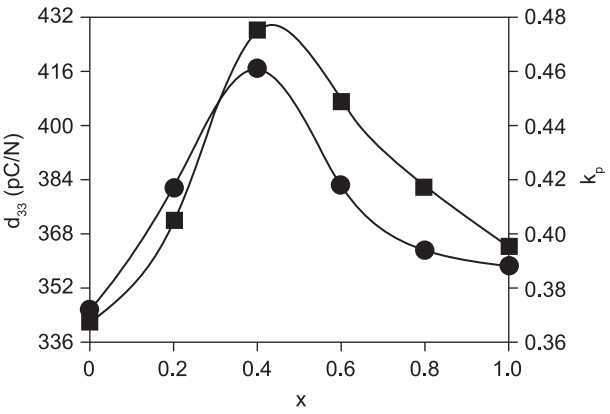

Figure 5. Piezoelectric properties of (1-x)(0.5PMN-0.5PZT) -xPBLBiN nanoceramic composites.

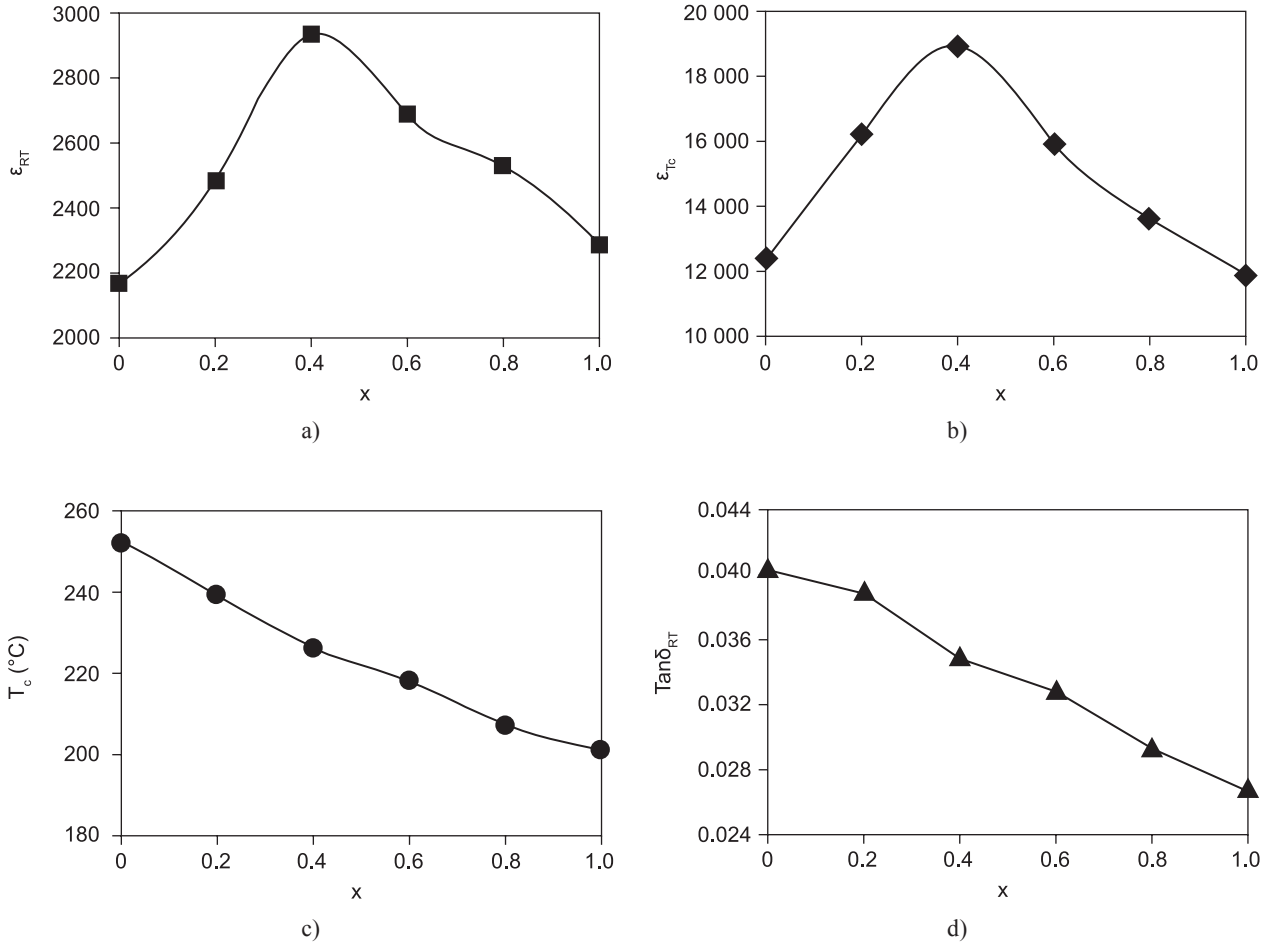

Figure 4. Dielectric properties of (1-x)(0.5PMN-0.5PZT)-xPBLBiN nanoceramic composites.

in A-sites and B-sites. Due to the coexistence of both 180° and 90° domains in the Pb-rich orthorhombic phase and rare-earth trivalent La can be accredited to increased piezoelectricity. We have observed from our previous investigations and present study that the electrical properties of the ceramic composites strongly depend on the: (i) stoichiometric ratios, (ii) the synthesis route/techniques followed and (iii) sintering conditions. Consecutively, the mechanism influencing inter and intra structural relationship between phase-formation, microstructure and density had a significant impact on the piezoelectric properties [13]. It is reported that in PMN-base solid solution ceramics, the effect of W^{6+} dopant resulted in pyrochlore phase and the dielectric and piezoelectric properties deteriorated [20]. However, in our study only two phases were evident; perovskite Cubic and tungsten bronze orthorhombic phase in (1-x)(0.5PMN-0.5PZT)-xPBLBiN nanoceramic composites. We consider that two effect factors act together to cause the enhanced piezoelectric properties for (1-x)(0.5PMN-0.5PZT)-xPBLBiN nanoceramic composites. One is La^{3+} doping resulting in the development of soft piezoelectric behavior; the other is the formation of binary phases. The piezoelectric properties were optimum at x = 0.4 that could be suitable for possible electromechanical and energy harvesting applications.

CONCLUSION

Perovskite-tungsten bronze structured ceramics exhibit high dielectric and electromechanical properties. In order to prepare the ceramics with excellent properties, proper content of substitute should be doped in the base composition. Investigations of the effect of La doping in xPBBiN in(1-x)(0.5PMN-0.5PZT)-xPBLBiN nanoceramic composites synthesized through mechanical activation method on structural and functional properties are reported. The milling process was optimized with 20 h at a speed of 250 rpm through Fritsch Pulverisette high energy mechanical activation technique. The ferroelectric complex nanoceramic composites in which La addition to xPBBiN demonstrated both perovskite cubic and tungsten bronze orthorhombic phases coexisted were successfully prepared in-situ which showed both compositional and microstructural homogeneity. The maximum dielectric constant (e_{RT} = 2931), piezoelectric planar coupling coefficient (k_p = 0.461) and the piezoelectric charge coefficient (d_{33} = 428 pC/N) was observed for x = 0.4 nanoceramic composite processed through non-conventional synthesis by mechanical activation (MA) technique that could be suitable for possible electromechanical and energy harvesting applications.

Acknowledgements

This work has been supported by the research grant funded by Fondecyt (Fondo Nacional de Desarrollo Científico y Tecnológico, Chile) through research project N°1080635. The authors would like to thank University of Concepcion, Chile and Andhra University, India for their collaboration and support extended. The authors would also like to thank Mr. Ranganathan, Mr. Krishnamurthy and Ms. C. N. Devi for their technical assistance and valuable suggestions extended during this work.

References

1. Oliver J.R., Neurgaonkar R.R., Cross L.E.: J. Am. Ceram. Soc. *72*, 202 (1989).
2. Burns G., Dacol F. H., Guo R., Bhalla A.S.: Appl. Phys. Lett. *57*, 543 (1990).
3. Lee M., Feigelson R.S.: J. Mater. Res. 13, 1345 (1998).
4. Guo R, Bhalla A.S., Randall C.A., Chang Z.P., Cross L.E.: Ferroelectrics *93*, 193 (1989).
5. Yu T., Shen Z.X., Xue J.M., Wang J.: Mater. Chem. Phys. *75*, 216 (2002).
6. Kong L.B., Ma J., Zhu W., Tan O.K.: J. Alloys. Comp. *322*, 290 (2001).
7. Wang J., Wan D.M., Xue J.M., Ng W.G.: J. Am. Ceram. Soc. *82*, 477 (1999).
8. Ang S.K., Xue J.M., Wang J.: J. Alloys. Comp. *343*, 156 (2002).
9. Ng S.H., Xue J.M., Wang J.: J. Am. Ceram. Soc. *85*, 2660 (2002).
10. Van H., Groen W.A., Maassen S., Keur W.C.: J. Eur. Ceram. Soc. *21*, 1689 (2001).
11. Kong L.B., Ma J., Zhu W., Tan O.K.: J. Mater. Sci. Lett. *20*, 1241 (2001).
12. Kong L.B., Ma J., Zhu W., Tan O.K.: Mater. Res. Bull. *37*, 23 (2002).
13. Ramam K., Lopez M., Chandramouli K.: J. Mater. Sci: Mater. Electron. *21*, 932 (2010).
14. Nagata K., Kawatani Y., Okazaki K.: Jap. J. Appl. Phys. *22*, 1353 (1983).
15. Neurgaonkar R.R., Oliver J.R., Nelson J.G., Cross L.E.: Mat. Res. Bull. *28*, 771 (1991).
16. Randall C.A., Guo R., Bhalla A.S., Cross L.E.: J. Mater. Res. *6*, 1720 (1991).
17. Kim M.S., Oh C.D., Lee J.H., Kim J.J., Lee H.Y., Cho S.H.: Ferroelectrics *334*, 105 (2006).
18. Wang P., Lee J.H., Kim J.J., Cho S.H., Lee H.Y.: Intl. J. of Modern Phys. B *17*, 1273 (2002).
19. Chen J., Chan H.M., Harmer M.P.: J. Am. Ceram. Soc. *72*, 593 (1989).
20. Zhong N., Dong X.L., Sun D.Z., Xiang P.H., Du H.: Mater. Res. Bull. *39*, 175 (2004).